ACS APPLIED MATERIALS & INTERFACES

Research Article

www.acsami.org

Highly Oriented Gold/Nanoclay–Polymer Nanocomposites for Flexible Gas Barrier Films

Eun-Ho Song,[†] Byung-Hyun Kang,[†] Tan-Young Kim,[†] Hyun-Jun Lee,[†] Young-Wook Park,[‡] Young-Cho Kim,*[,§] and Byeong-Kwon Ju*[,†]

[†]Display and Nanosystem Laboratory, College of Engineering, and [‡]The Institute of High Technology Materials and Devices, Korea University, Seoul 136-713, Republic of Korea

[§]Advanced Information Display Laboratory, College of Engineering, Chungwoon University, Incheon, 402-803, Republic of Korea

Supporting Information

ABSTRACT: Layer-by-layer (LBL) assembly, which uses electronic and ionic intermolecular bonding under nonvacuum conditions, is a promising technology for fabricating gas barrier films owing to its simple processing and easy formation of a multilayer structure. In this research, nanoclay–polymer multilayers of Na^+-montmorillonite (Na-MMT) were fabricated. Particularly, the addition of $AuCl_3$ on fabricated MMT layers caused a reaction with the surface silanol functional groups (Si–O–H) of the MMT platelets, resulting in the formation of Au_2O_3 on the MMT–polymer multilayers. The Au_2O_3 filled the vacancies between the MMT platelets and linked the MMT platelets together, thus forming a gas barrier film that reduced the water vapor transmission rate (WVTR) to 3.2×10^{-3} g m^{-2} day^{-1}. $AuCl_3$-treated MMT–polymer multilayers thus have the potential to be utilized for manufacturing gas barrier films for flexible electronics on a large scale.

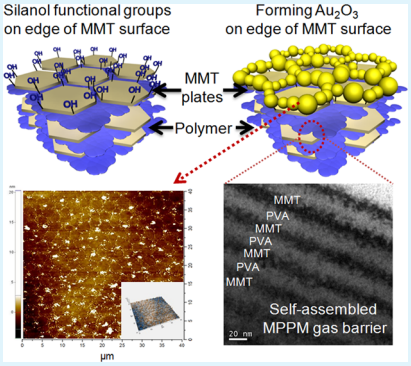

KEYWORDS: *flexible gas barrier films, nanoclay, 2D materials, gold complex, water vapor transmission rate*

1. INTRODUCTION

Flexible electronics are the next generation of electronics, and their development requires the fabrication of flexible gas barrier films in order to prevent oxidation of the devices. Such films generally consist of an inorganic/organic multilayer structure.[1−3] The multilayer structure causes transmitted water vapor to move horizontally on each of the inorganic layers until it encounter defects of inorganic layer, rather than vertically pass through the gas barrier film. The effective thickness of the gas barrier film is thus enlarged using a multilayer structure. This is important because completely adsorbed water vapor reacts electrochemically with the cathode (which is generally made of aluminum), forming additional H_2 gas inside the device. In addition, unreacted water vapor penetrates the bottom layer of the cathode. This H_2 or transmitted water vapor forms bubbles at the cathode, which destroys the devices.[4] The rate at which water vapor passes through the gas barrier film is called the water vapor transmission rate (WVTR). Thus, the WVTR is considered to be a significant property because transmitted water vapor destroys devices. For this reason, multilayer gas barrier films are constructed to reduce the WVTR value.[5−7] Vacuum-based processes such as chemical vapor deposition, atomic layer deposition, and sputtering are generally used for fabricating such multilayer structures. However, vacuum-based processing has disadvantages in terms of low production efficiency and high production costs.

Recently, there has been increased interest in fabricating gas barrier films using nonvacuum processes. Among the processes available, layer-by-layer (LBL) assembly, which leads to the self-assembly of multilayer structures, has received much attention.[8−13] In LBL assembly, the multilayer thin film is constructed by alternately dipping a substrate into aqueous cationic and anionic mixtures. LBL assembly has advantages in terms of easily constructing multilayer structures and controlling the film thickness by cycle modification in nonvacuum conditions. In addition, the surface properties of each layer of the fabricated film are easily controlled by modulating the ionic strength, which can be performed by adjusting the pH of each aqueous dipping solution.[14,15] A variety of materials have been used in the LBL process, although aqueous charged nanosheets are the most widely reported.[16−18]

To fabricate a gas barrier film by LBL assembly, researchers have usually used montmorillonite (MMT, nanoclay), graphene oxide (GO), and two-dimensional inorganic materials in the form of aqueous dispersions as the negatively charged materials,[8,10,13] whereas aqueous solutions/dispersions of polyethylenimine, poly(diallyldimethylammonium chloride) (PDDA), and other organic materials have been used as the positively charged materials.[16,17] MMT has been researched as

Received: December 8, 2014
Accepted: February 10, 2015
Published: February 10, 2015

DOI: 10.1021/am508641g
ACS Appl. Mater. Interfaces 2015, 7, 4778−4783

a gas barrier film material because of its easy dispersion in water and its transparent properties. Furthermore, gas barrier films, which composed of MMT, shows low WVTRs of <0.05 g m^{-2} day^{-1}.[8,9,16] However, functional groups on the MMT platelet surface such as silanol groups (Si−O−H) play an important role.[19] These functional groups make the gas barrier film surface hydrophilic, leading to the deterioration of the gas barrier film properties by facilitating the transmission of water vapor through the fabricated MMT gas barrier films.

In this study, we applied bonded stable materials to the silanol functional groups present on the MMT surfaces to modify the surface characteristics of the gas barrier films. Especially, a gold(III) chloride ($AuCl_3$) solution was used to react with the silanol functional groups on the MMT surface. Previous studies have shown that gold complexes can be used to modify the surface properties by oxidation with surface functional groups.[20−23] In this research, the $AuCl_3$ solution was drop-casted on the MMT multilayer surface, leading to the formation of gold oxide (Au_2O_3) on the MMT multilayer surface. As a result, this simple treatment significantly enhances the gas-barrier film properties.

2. EXPERIMENTAL SECTION

2.1. Gas Barrier Film Fabrication. Na^+-MMT (purchased from Southern Clay Products, US) was used as the anionic material [forming a negatively charged dispersion in deionized (DI) water]. A mixture of 1 wt % MMT in 150 mL of DI water was magnetically stirred for 24 h to disperse the MMT uniformly. The uniformly dispersed MMT solution was centrifuged for 1 h at 83 s^{-1} to separate large precipitated MMT platelets from small MMT platelets to maximize horizontal water vapor transmission path. After the first centrifugation, the large precipitated MMT particles were separated and again dispersed in 150 mL of DI water. This precipitated MMT solution was magnetically stirred for 24 h to uniformly disperse the MMT particles. Next, solutions of well-dispersed large MMT particles (precipitated MMT particles after the first centrifugation) were centrifuged at 28 s^{-1} for 15 min to extract the unaggregated MMT particles. As output of the second centrifugation, MMT particles floating in the precipitated MMT solution were separated and this floating MMT solution was magnetically stirred for 24 h, resulting in MMT particles 2−4 μm in size (see the Supporting Information). Next, a solution of 0.5 wt % of PVA (M_w = 30 000−70 000, 87−90% hydrolyzed, purchased from Sigma-Aldrich) in DI water was prepared. The previously prepared MMT solution (final output of double centrifugation) and PVA solution were mixed in a ratio of 4:1 by volume and magnetically stirred for 24 h in order to adsorb the PVA between the MMT layers in the solution. The pH of the MMT(PVA) solution was adjusted to 3 by adding 1 M HCl solution. PDDA (M_w = 200 000−350 000, 20 wt % H_2O, purchased from Sigma-Aldrich) was used as the cationic material, which formed a positively charged solution in DI water. PDDA (2 wt %) in DI water was magnetically stirred for 24 h and the pH of the PDDA solution was adjusted to 10 by adding 1 M NaOH solution. A cleaned polyethylene naphthalate (PEN, purchased from DuPont Teijin, thickness 125 μm) substrate was exposed for 20 min to a UV-ozone lamp to form a negatively charged PEN surface. The substrate was alternately dipped in the prepared PDDA and MMT(PVA) mixtures, each for 10 min. After each dipping of the substrate in the PDDA and MMT(PVA) mixtures, the substrate was rinsed three times in pure DI water for 1 min. As a result, an MMT(PVA)−PDDA multilayer (MPPM) film was achieved. One of the fabricated MPPM films was treated with $AuCl_3$ (M_w = 303.33, purchased from Sigma-Aldrich). A solution of $AuCl_3$ (0.1 wt %) in nitromethane was drop-casted onto the fabricated MPPM film for 1 min. The remaining $AuCl_3$ solution was removed by air gun blowing. Subsequently, the fabricated gas-barrier film was dried for 60 min at 120 °C on a hot plate.

2.2. Electrical Ca-Test for WVTR Measurement. The gas-barrier film properties were evaluated by measuring the WVTR using the previously reported electrical Ca-test.[24,25] The electrical Ca-test is a simple and convenient system for measuring the WVTR. Moreover, it can be used to measure WVTR over a wide range of 100−10^{-6} g m^{-2} day^{-1}.[24,25] Because of these advantages, the electrical Ca-test has been used widely for WVTR measurements of gas-barrier films.[6,17,26]

In this system, the amount of water vapor transmitted through a gas barrier film can be detected by a Ca sensor. Ca degenerates to form calcium oxide upon reaction with the transmitted water vapor. The degree of Ca oxidation is then monitored by resistance measurements. In this research, a constant voltage of 5 mV was applied to the Ca sensor to monitor calcium degradation (see the Supporting Information). The reliability of the Ca-test was verified by comparing it with the commercialized permeability measurement system MOCON. The WVTR values measured by electrical Ca-test and the MOCON system were similar (see the Supporting Information).

2.3. Analysis Using XPS, SEM, TEM, AFM, and UV−Vis Spectrophotometer. X-ray photoelectron spectroscopy (XPS) signals were recorded using a PHI X-tool system equipped with a monochromatic Al X-ray source (1486.6 eV). The X-ray beam diameter was 106.2 μm. The untreated and $AuCl_3$-treated MPPM films were analyzed in order to confirm the oxide bonding structures. The O 1s and Au 4f binding energies in particular were analyzed. Scanning electron microscopy (SEM, Hitachi S-4300, Hitachi) and transmission electron microscopy (TEM, Tecnai 20, FEI Tecnai) were used for identifying the micro- and nanosized structure of the MPPM films. For SEM analysis, Thin Pt layer was coated on the MPPM films to obtain clear images. For cross-sectional TEM analysis, the focused ion beam technique (FIB, LYRA3 XMH, TESCAN) was used for preparing cross-sectional specimens of the MPPM films. A Pt sacrificial layer was deposited on the MPPM films. After FIB sampling, specimens were transferred to the TEM grid. The TEM observations were performed using a Tecnai 20 instrument operated at 200 kV to enhance the contrast between MPPM films. Moreover, atomic force microscopy (AFM, XE 100, Park Systems) was used for scanning 40 μm × 40 μm regions of the MPPM film surface. The light transmittance of the MPPM films was measured using a UV−vis spectrophotometer (Cary 5000, Varian Instruments). The UV−vis spectrophotometer exposed the untreated and $AuCl_3$-treated MPPM films to the visible regions of the electromagnetic spectrum (350−700 nm) when the films were placed in a UV−vis beam. The amount of light that was not absorbed and passed through the MPPM film to the detector depended upon the properties of the films (see the Supporting Information).

2.4. Contact-Angle Measurement. A contact-angle analyzer (BS 150, Surface Tech) was used for measuring the contact angle between a DI water droplet and the surface of the MPPM film. A droplet of DI water was carefully dropped onto each untreated and $AuCl_3$-treated MPPM film through a syringe. The contact angle measuring stand was carefully adjusted to ensure a flat surface.

3. RESULTS AND DISCUSSION

The structure of the MPPM film and the LBL self-assembly methods are shown in panels a and b in Scheme 1, respectively. The MMT layers mixed with poly(vinyl alcohol) (PVA) and PDDA layers were alternately stacked 10 times.

The thicknesses of the untreated and $AuCl_3$-treated MPPM films were measured as 4 μm, as shown in Figure 1a, b. We were able to fabricate the thick multilayer by controlling the pH. Interestingly, the total thicknesses of the untreated and $AuCl_3$-treated films were similar because the reaction between $AuCl_3$ and MMT partially occurred on the surface edges of the MMT platelets, which is where the silanol functional groups (Si−O−H) are located.[19] The surface roughness increased slightly in the case of the $AuCl_3$-treated MPPM film because of the formation of Au_2O_3. Figure 1c, d show cross-sectional HR-TEM images of the untreated and $AuCl_3$-treated MPPM films, respectively. The alternating structure of MMT and PVA can be

DOI: 10.1021/am508641g
ACS Appl. Mater. Interfaces 2015, 7, 4778−4783

Scheme 1. (a) Structure of the Fabricated MPPM Film; One of the Fabricated MPPM Films Was Treated with $AuCl_3$ and the Other Was Left Untreated; (b) Sequence of Fabrication of the MPPM Film by the LBL Process

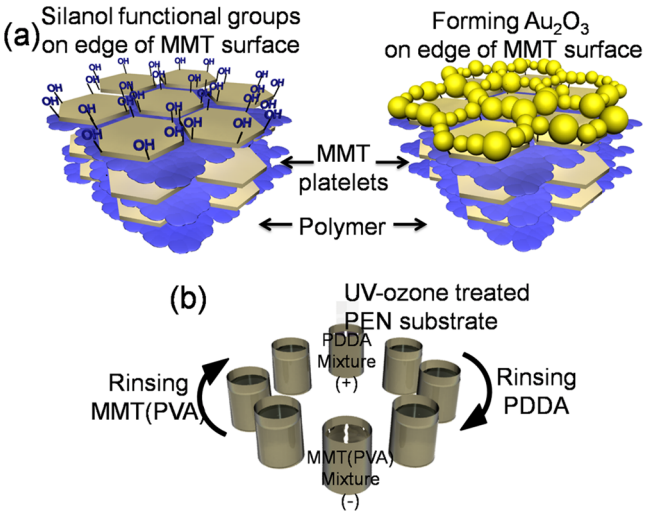

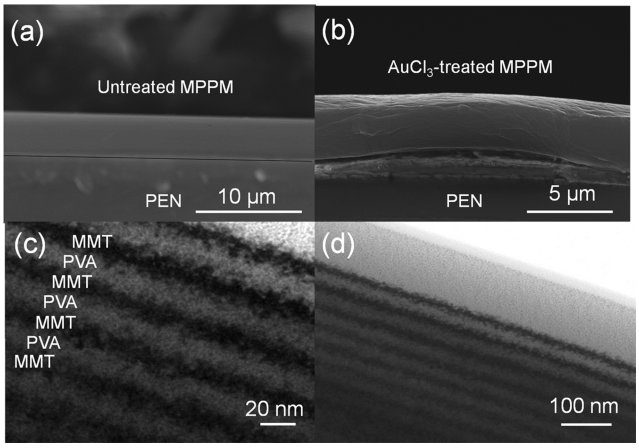

Figure 1. Cross-sectional SEM image of the (a) untreated MPPM film and (b) $AuCl_3$-treated MPPM film. Cross-sectional HR-TEM image of (c) untreated and (d) $AuCl_3$-treated MPPM film.

clearly identified. As mentioned previously, since weakly aggregated MMT was extracted during centrifuging, thick layers formed between each of the MMT and PVA layers. Moreover, Figure 1c, d shows the $AuCl_3$ reaction region of the MMT−PDDA multilayer. Although Figure 1d shows a cross-sectional image of the $AuCl_3$-treated MPPM film, granular Au_2O_3 could not be seen in the interlayers of the MPPM film. Therefore, it can be concluded that the reaction between $AuCl_3$ and MPPM film occurred mainly on the surface of the gas-barrier film.

The water vapor transmission rate (WVTR) of the fabricated gas-barrier films was evaluated by electrical Ca-tests (see the Supporting Information). In this system, Ca was thermally evaporated for use as a water vapor-detecting sensor. Ca (metal) is degraded to form calcium oxide (ceramic) by reacting with water vapor. Utilizing this property, the electrical Ca-test measures the degree of degradation in the calcium conductivity resulting from this reaction.[24,25] As shown in Figure 2a, the WVTR of the untreated MPPM film was 2.0×10^{-2} g m^{-2} day^{-1}, whereas that of the $AuCl_3$-treated MPPM

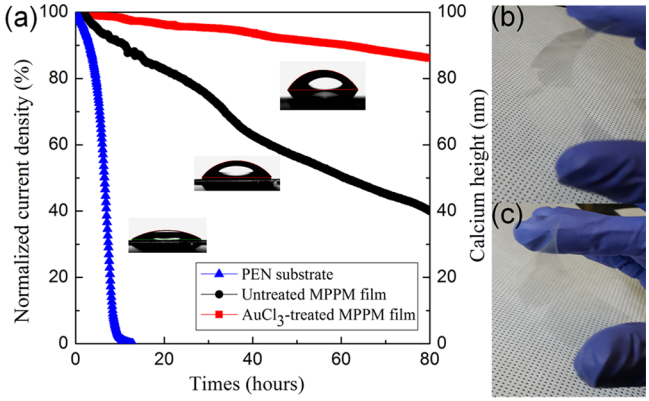

Figure 2. (a) WVTR results. Red square line shows WVTR values for the $AuCl_3$-treated MPPM film, whereas the black circle line shows WVTR values of the untreated MPPM film. The contact-angle images of each sample are also shown. Images of (b) untreated and (c) $AuCl_3$-treated MPPM film.

film was measured to be 3.2×10^{-3} g m^{-2} day^{-1}. Hence, the amount of transmitted water vapor through the $AuCl_3$-treated MPPM film was greatly reduced. Furthermore, as shown in Figures 2b, c, the gas-barrier film was perfectly transparent.

These results indicate that water vapor easily penetrated the untreated MPPM film via vacancies between the MMT platelets. In contrast, water vapor transmission was restricted with the $AuCl_3$-treated MPPM film. This improvement can be attributed to Au_2O_3 formation caused by the reaction between silanol functional groups on the MMT surface and $AuCl_3$. Furthermore, the formed Au_2O_3 links adjacent MMT platelets together because one Au^{3+} ion can react with several functional groups. In this work, this is called the bridging effect. This bridging effect prevents water vapor penetration by filling vacancies between the MMT platelets. Also, it modifies the surface properties and renders the surface slightly hydrophobic, as found from the contact-angle measurements (see the Supporting Information).[27,28] The contact angle of the $AuCl_3$-treated MPPM film was 53°, whereas the contact angle of the untreated MPPM film was 40°. The surface energies calculated by Owen's law were determined to be 43 and 56 mN/m for the $AuCl_3$-treated and untreated MPPM films, respectively. These results show that the surface energy was reduced because the formation of Au_2O_3 on the surface reduced the number of functional groups on the MMT surface, rendering the surface slightly hydrophobic.

To ensure the formation of Au_2O_3 on the MPPM film, SEM-EDX was used for analyzing the elemental composition. As shown in Figure 3, the increase in the O and Au peak intensities indicate the formation of Au_2O_3. In the EDX spectrum, though the Au peak could not be clearly distinguished because it had a peak position similar to that of Si, the O peak intensity shown in Figure 3b, dramatically increased as compared to that in Figure 3a, indicating oxide formation. In addition, as shown in Figure 3c, d, granular Au_2O_3 was partially formed on the MMT surface, and the number of grain boundaries decreased. These figures indicate that the formed Au_2O_3 was partially formed on the clay platelets, rather than forming a uniformly layered structure. Partially formed Au_2O_3 effectively fills vacancies between the MMT platelets by reacting with silanol functional groups that exist on the edges of MMT platelets. For this reason, partially formed granular Au_2O_3 was able to prevent water vapor transmission through the vacancies in the MPPM

DOI: 10.1021/am508641g
ACS Appl. Mater. Interfaces 2015, 7, 4778−4783

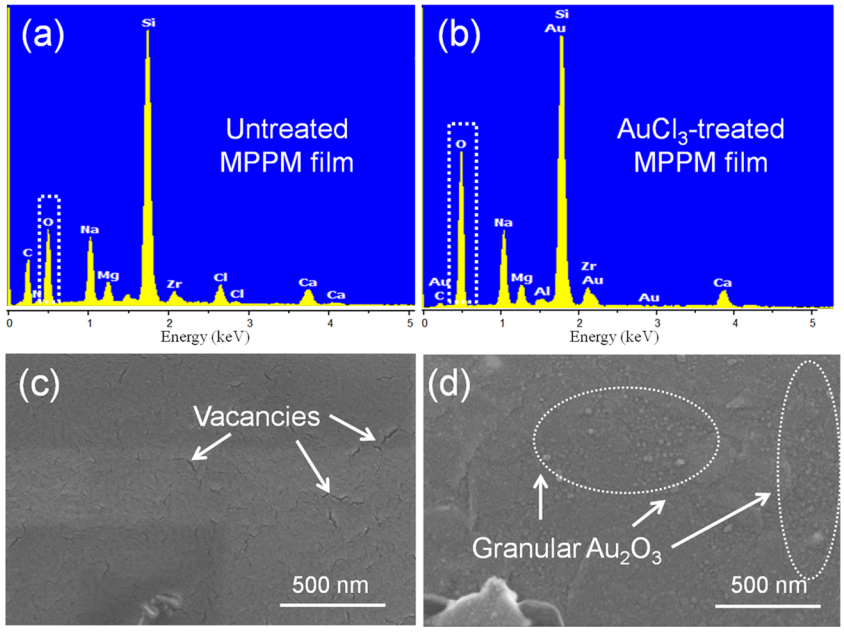

Figure 3. EDX results for (a) untreated and (b) $AuCl_3$-treated MPPM film. SEM surface images of (c) untreated and (d) $AuCl_3$-treated MPPM film.

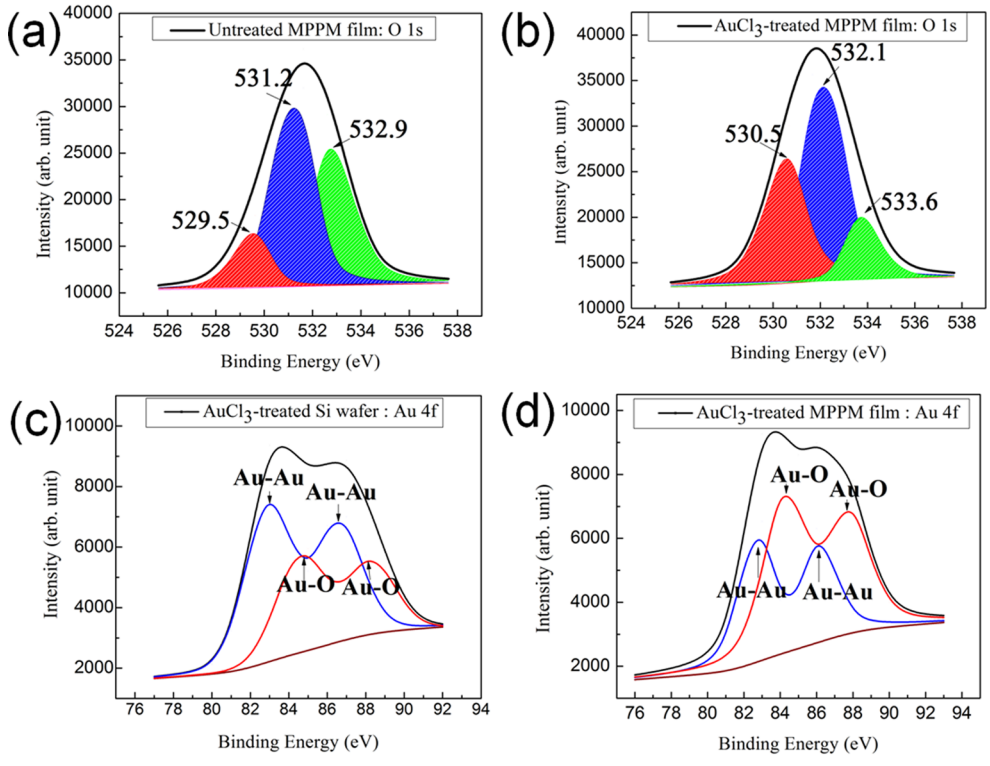

Figure 4. O 1s binding energy distribution for (a) untreated and (b) $AuCl_3$-treated MPPM film. Distribution of the Au 4f peak when $AuCl_3$ solution was drop-casted on a (c) bare Si wafer and (d) MPPM film.

film. X-ray photoelectron spectroscopy (XPS) was performed to investigate the binding structure between Au_2O_3 and MMT. All the C 1s binding energies were fixed at 284.6 eV. The bond structure of the oxide groups was identified by O 1s binding energy analysis. Figure 4a, b shows the O 1s binding energy of each sample. The $AuCl_3$-treated MPPM film with Au_2O_3 on the surface showed increased intensity of the 539.5 eV peak, which is related to the formation of Au_2O_3.[29,30] Moreover, Figure 4b shows that the intensity of the peak at 533 eV, which denotes the oxygen in water molecules, decreased when Au_2O_3 was formed on the MMT surface in comparison to the peak intensity of the untreated MPPM film.[31] This could be explained on the basis that functional groups on the MMT surface attract water vapor. When the MMT surface was treated with $AuCl_3$; however, functional groups reacted with $AuCl_3$ and formed Au_2O_3. In summary, the O 1s peak analysis results indicate that in the case of the $AuCl_3$-treated MPPM film, Au_2O_3 formed on the edges of the MMT platelets, which linked

DOI: 10.1021/am508641g
ACS Appl. Mater. Interfaces 2015, 7, 4778−4783

the MMT platelets. This bridging effect could also be confirmed through analysis of the Au 4f peaks. Figure 4c, d shows the Au 4f peaks obtained from the $AuCl_3$-treated and untreated MPPM film fabricated on Si wafers, respectively. The Au−O peak intensity was higher than the Au−Au peak intensity in the case of the $AuCl_3$-treated MPPM film, which indicates that Au_2O_3 was chemically adsorbed by reacting with the functional groups on the MMT platelets.[32]

Atomic force microscopy (AFM) also confirmed the results obtained by XPS. As shown in Figure 5, granular Au_2O_3 formed

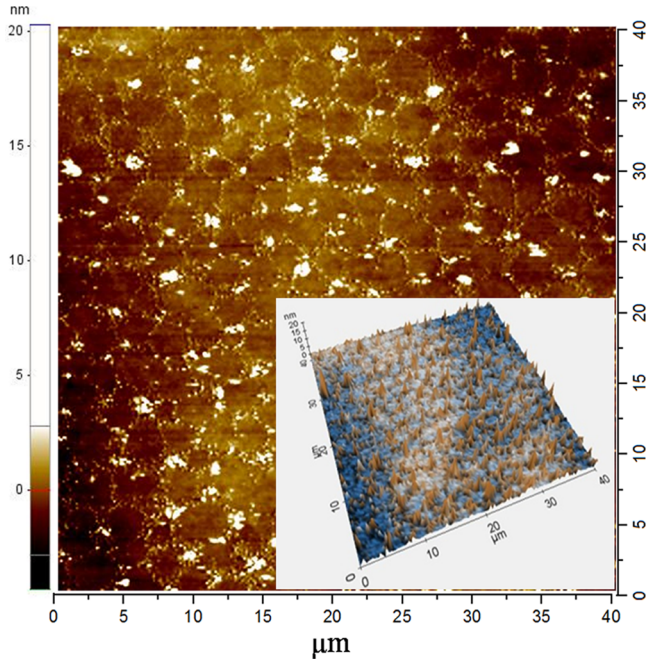

Figure 5. AFM image of 40 × 40 μm area, which clearly indicates the formation of Au_2O_3 on the edge of each of the MMT platelet.

on the MMT grain boundaries, confirming that Au^{3+} ions bound with the functional groups present on the edges of the MMT platelets and that Au_2O_3 formed, linking the MMT platelets and filling the vacancies between the platelets. In addition, this figure clearly shows that granular Au_2O_3 partially formed on the surface of the MPPM films, especially on the edges of the MMT platelets, rather than forming a uniform Au_2O_3 layer.

The light transmittances of the fabricated gas barrier films were analyzed by an ultraviolet- visible spectrophotometer (in particular, we used the wavelength range 200−800 nm). At 550 nm, the light transmittance of the untreated MPPM film was measured as 99% in comparison to the PEN substrate (see the Supporting Information, Figure 2b). The $AuCl_3$-treated MPPM film showed a light transmittance of 98% at 550 nm, as shown in Figure 2c.

4. CONCLUSION

Gas-barrier films using MMT as the inorganic material contain silanol functional groups on the surfaces of the MMT platelets and are hydrophilic, which are disadvantages in terms of the gas-barrier film properties. To solve these problems, in this study, we drop-casted $AuCl_3$ onto a MMT(PVA)-PDDA multilayer film (MPPM film), which resulted in the formation of Au_2O_3. Au_2O_3 caused a bridging effect, in which Au_2O_3 linked the MMT platelets together and prevented the permeation of water vapor through the gas barrier film. Furthermore, the $AuCl_3$ treatment rendered the film surface more hydrophobic and improved the WVTR. This newly designed $AuCl_3$-treated MPPM film is simple, safe, and effective and provides a promising alternative to the production of high-quality nanocomposite gas barrier films. These are the initial results of a novel method of chemical treatment on MMT nanocomposite for gas barrier film applications. We expect that the method of gas barrier film fabrication proposed here, which does not require vacuum conditions, can be applied to the production of flexible electronics on a large scale.

■ ASSOCIATED CONTENT

Supporting Information

Material preparation, MMT particle size measurement, light transmittance measurement, water vapor transmission rate (WVTR) measurement (electrical Ca-test), contact angle measurement, and XPS binding energy analysis. This material is available free of charge via the Internet at http://pubs.acs.org.

■ AUTHOR INFORMATION

Corresponding Authors

*E-mail: yckim@chungwoon.ac.kr.
*E-mail: bkju@korea.ac.kr.

Author Contributions

The manuscript was written through contributions of all authors. All authors have given approval to the final version of the manuscript. B.-K.J. planned the entire research. Y.-C.K. and Y.-W.P. advised authors on analyzing techniques. B.-H.K., E.-H.S., H.-J.L. analyzed the results. E.-H.S. and T.-Y.K. fabricated the gas barrier films.

Notes

The authors declare no competing financial interest.

■ ACKNOWLEDGMENTS

This work was supported by the RFID R&D program of MKE/KEIT [10035225, Development of Core Technology for High-performance AMOLED on Plastic]. Also, this research was supported by Academic Research Foundation of Chungwoon University (2013). The authors thank the staff of Korea Basic Science Institute (KBSI) and Korea Institute of Science and Technology (KIST) for technical assistance.

■ REFERENCES

(1) Meyer, J.; Schmidt, H.; Kowalsky, W.; Riedl, T.; Kahn, A. The Origin of Low Water Vapor Transmission Rates through Al_2O_3/ZrO_2 Nanolaminate Gas-diffusion Barriers Grown by Atomic Layer Deposition. *Appl. Phys. Lett.* **2010**, *96*, 243308.

(2) Lewis, J. S.; Weaver, M. S. Thin-film Permeation-barrier Technology for Flexible Organic Light-Emitting Diodes. *IEEE. J. Sel. Top. Quantum Electron.* **2004**, *10*, 45−57.

(3) Langereis, E.; Creatore, M.; Heil, S. B. S.; van de Sanden, M. C. M.; Kessels, W. M. M. Plasma-assisted Atomic Layer Deposition of Al_2O_3 Moisture Permeation Barriers on Polymers. *Appl. Phys. Lett.* **2006**, *89*, 081915.

(4) Schaer, M.; Nuesch, F.; Berner, D.; Leo, W.; Zuppiroli, L. *Adv. Funct. Mater.* **2001**, *11*, 116−121.

(5) Choi, J. H.; Kim, Y. M.; Park, Y. W.; Park, T. H.; Jeong, J. W.; Choi, H. J.; Song, E. H.; Lee, J. W.; Kim, C. H.; Ju, B. K. Highly Conformal SiO_2/Al_2O_3 Nanolaminate Gas-diffusion Barriers for Large-area Flexible Electronics Applications. *Nanotechnology* **2010**, *21*, 475203.

(6) Chwang, A. B.; Rothman, M. A.; Mao, S. Y.; Hewitt, R. H.; Weaver, M. S.; Silvernail, J. A.; Rajan, K.; Hack, M.; Brown, J. J.; Chu,

DOI: 10.1021/am508641g
ACS Appl. Mater. Interfaces 2015, 7, 4778−4783

X.; More, L.; Krajewski, T.; Rutherford, N. Thin Film Encapsulated Flexible Organic Electroluminescent Displays. *Appl. Phys. Lett.* **2003**, *83*, 413−415.
(7) Tropsha, Y. G.; Harvey, N. G. Activated Rate Theory Treatment of Oxygen and Water Transport Through Silicon Oxide/Poly(ethylene terephthalate) Composite Barrier Structures. *J. Phys. Chem. B* **1997**, *101*, 2259−2266.
(8) Priolo, M. A.; Gamboa, D.; Holder, K. M.; Grunlan, J. C. Super Gas Barrier of Transparent Polymer-Clay Multilayer Ultrathin Films. *Nano Lett.* **2010**, *10*, 4970−4974.
(9) Walther, A.; Bjurhager, I.; Malho, J. M.; Pere, J.; Ruokolainen, J.; Berglund, L. A.; Ikkala, O. Large-Area, Lightweight and Thick Biomimetic Composites with Superior Material Properties via Fast, Economic, and Green Pathways. *Nano Lett.* **2010**, *10*, 2742−2748.
(10) Kunz, D. A.; Schmid, J.; Feicht, P.; Erath, J.; Fery, A.; Breu, J. Clay-Based Nanocomposite Coating for Flexible Optoelectronics Applying Commercial Polymers. *ACS Nano* **2013**, *7*, 4275−4280.
(11) Holder, K. M.; Priolo, M. A.; Secrist, K. E.; Greenlee, S. M.; Nolte, A. J.; Grunlan, J. C. Humidity-Responsive Gas Barrier of Hydrogen-Bonded Polymer-Clay Multilayer Thin Films. *J. Phys. Chem. C* **2012**, *116*, 19851−19856.
(12) Lutkenhaus, J. L.; McEnnis, K.; Hammond, P. T. Nano- and Microporous Layer-by-Layer Assemblies Containing Linear Poly-(ethylenimine) and Poly(acrylic acid). *Macromolecules* **2008**, *41*, 6047−6054.
(13) Decher, G.; Schlenoff, J. B. *Multilayer Thin Films: Sequential Assembly of Nanocomposite Materials*, 2nd ed; Wiley−VCH: Weinheim, Germany, 2012.
(14) Yoo, D.; Shiratori, S. S.; Rubner, M. F. Controlling Bilayer Composition and Surface Wettability of Sequentially Adsorbed Multilayer of Weak Polyelectrolytes. *Macromolecules* **1998**, *31*, 4309−4318.
(15) Poon, Zhiyong; Chang, D.; Zhao, X.; Hammond, P. T. Layer-by-Layer Nanoparticles with a pH-Sheddable Layer for in Vivo Targeting of Tumor Hypoxia. *ACS Nano* **2011**, *5*, 4284−4292.
(16) Choi, J. H.; Park, Y. W.; Park, T. H.; Song, E. H.; Lee, H. J.; Kim, H. K.; Shin, S. J.; Fai, V. L. C. F.; Ju, B. K. Fuzzy Nanoassembly of Polyelectrolyte and Layered Clay Multicomposite toward a Reliable Gas Barrier. *Langmuir* **2012**, *28*, 6826−6831.
(17) Yang, T. H.; Bolling, L.; Priolo, M. A.; Grunlan, J. C. Super Gas Barrier and Selectivity of Graphene Oxide-Polymer Multilayer Thin Films. *Adv. Mater.* **2013**, *25*, 503−508.
(18) Ning, W.; Xingxiang, Z.; Na, H.; Shihe, B. Effect of Citric Acid and Processing on the Performance of Thermoplastic Starch/Montmorillonite Nanocomposites. *Carbohydr. Polym.* **2009**, *76*, 68−73.
(19) Mansoori, Y.; Atghia, S. V.; Zammanloo, M. R.; Imanzadeh, Gh.; Sirousazar, M. Polymer-clay Nanocomposites: Free Radical Grafting of Polyacrylamide onto Organophilic Montmorillonite. *Eur. Polym. J.* **2010**, *46*, 1844−1853.
(20) Kim, S. M.; Kim, K. K.; Jo, Y. W.; Park, M. H.; Chae, S. J.; Duong, D. L.; Yang, C. W.; Kong, J.; Lee, Y. H. Role of Anions in the $AuCl_3$-Doping of Carbon Nanotubes. *ACS Nano* **2011**, *5*, 1236−1242.
(21) Lu, X.; Yavuz, M. S.; Tuan, H. Y.; Korgel, B. A.; Xia, Y. Ultrathin Gold Nanowires Can Be Obtained by Reducing Polymeric Strands of Oleylamine-AuCl Complexes Formed via Aurophilic Interaction. *J. Am. Chem. Soc.* **2008**, *130*, 8900−8901.
(22) Chen, A.; Lipkowski, J. Electrochemical and Spectroscopic Studies of Hydroxide Adsorption at the Au(111) Electrode. *J. Phys. Chem. B* **1999**, *103*, 682−691.
(23) Cuenya, B. R.; Baeck, S. H.; Jaramillo, T. F.; McFarland, E. W. Size- and Support-Dependent Electronic and Catalytic Properties of Au^0/Au^{3+} Nanoparticles Synthesized from Block Copolymer Micelles. *J. Am. Chem. Soc.* **2003**, *125*, 12928−12934.
(24) Choi, J. H.; Kim, Y. M.; Park, Y. W.; Huh, J. W.; Kim, I. S.; Hwang, H. N.; Ju, B. K. Evaluation of Gas Permeation Barrier Properties Using Electrical Measurements of Calcium Degradation. *Rev. Sci. Instrum.* **2007**, *78*, 064701.
(25) Song, E. H.; Park, Y. W.; Choi, J. H.; Park, T. H.; Jeong, J. W.; Choi, H. J.; Ju, B. K. The Flexible Ca-test: An Improved Performance in a Gas Permeability Measurement System. *Rev. Sci. Instrum.* **2011**, *82*, 0547.
(26) Seo, S. W.; Jung, Eun.; Seo, S. J.; Chae, H. Y.; Chung, H. K.; Cho, S. M. Toward Fully Flexible Multilayer Moisture-Barrier s for Organic Light-Emitting Diodes. *J. Appl. Phys.* **2013**, *114*, 143505.
(27) Owens, D. K. Estimation of the Surface Free Energy of Polymers. *J. Appl. Polym. Sci.* **1969**, *13*, 1741−1747.
(28) Choi, J. H.; Kim, Y. M.; Park, Y. W.; Park, T. H.; Dong, K. Y.; Ju, B. K. Hydrophilic Dots on Hydrophobic Nanopatterned Surface as a Flexible Gas Barrier. *Langmuir* **2009**, *25*, 7156−7160.
(29) Pireaux, J. J.; Liehr, M.; Thiry, P. A.; Delrue, J. P.; Caudano, R. Electron Spectroscopic Characterization of Oxygen Adsorption on Gold Surfaces. *Surf. Sci.* **1984**, *141*, 221−232.
(30) Juodkazis, K.; Juodkazyte, J.; Jasulaitiene, V.; Lukinskas, A.; Sebeka, B. XPS Studies on the Gold Oxide Surface Layer Formation. *Electrochem. Commun.* **2000**, *2*, 503−507.
(31) Koslowski, B.; Boyen, H. G.; Wilderotter, C.; Kastle, G.; Ziemann, P.; Wahrenberg, R.; Oelhafen, P. Oxidation of Preferentially (111)-Oriented Au Films in an Oxygen Plasma Investigated by Scanning Tunneling Microscopy and Photoelectron Spectroscopy. *Surf. Sci.* **2001**, *475*, 1−10.
(32) Tsai, H.; Hu, E.; Perng, K.; Chen, M.; We, J. C.; Chang, Y. S. Instability of Gold Oxide Au_2O_3. *Surf. Sci.* **2003**, *537*, L447−L450.

DOI: 10.1021/am508641g
ACS Appl. Mater. Interfaces 2015, 7, 4778−4783